Main Manuscript for

Intermittent bulk release of human cytomegalovirus through multivesicular bodies

Felix J. Flomm[1,2,3,4], Timothy K. Soh[1,2,3,4], Carola Schneider[4], Hannah M. Britt[5], Konstantinos Thalassinos[5,6], Søren Pfitzner[4], Rudolph Reimer[4], Kay Grünewald[1,3,4,7], Jens B. Bosse[1,2,3,4]*

[1] Centre for Structural Systems Biology, Hamburg, Germany
[2] Hannover Medical School, Institute of Virology, Hannover, Germany
[3] Cluster of Excellence RESIST (EXC 2155), Hannover Medical School, Hannover, Germany
[4] Heinrich Pette Institute Leibniz-Institute for Experimental Virology, Hamburg, Germany
[5] Institute of Structural and Molecular Biology, Division of Biosciences, University College London, London, United Kingdom
[6] Institute of Structural and Molecular Biology, Birkbeck College, University of London, London, United Kingdom
[7] University of Hamburg, Department of Chemistry, Hamburg, Germany

*Jens B. Bosse, Center for Structural Systems Biology, Notkestraße 85, 22607 Hamburg

Email: jens.bernhard.bosse@cssb-hamburg.de

Felix J. Flomm: 0000-0001-7691-0519

Hannah M. Britt 0000-0001-8510-0331

Konstantinos Thalassinos 0000-0001-5072-8428

Kay Grünewald: 0000-0002-4788-2691

Jens B. Bosse: 0000-0001-7252-5541

Classification

Biological Sciences

Microbiology

Keywords

Human Cytomegalovirus, Integrative Microscopy, Viral egress, Morphogenesis

Author Contributions

Designed research: FJF, KT, RR, KG, JBB; Performed research: FJF, TKS, CS, HB, RR; Contributed new analytic tools: RR, CS, SP; Analyzed data: FJF, TKS, JBB; Wrote the paper: KG, FJF, TKS, JBB.

This PDF file includes:

Main Text
Figures 1 to 5
Tables 1
Supplementary Figures 1 to 2
Legends to Supplementary Videos 1A/B to 5 and Supplementary Table 1

Abstract

Human Cytomegalovirus (HCMV) is a highly prevalent herpesvirus that establishes lifelong latent infection in humans. It is the leading cause of congenital disabilities and a significant cause of disease in immunocompromised patients (1). HCMV significantly remodels host cell processes and membranes for the effective production of virus progeny (2). Their final morphogenesis process occurs in the cytoplasm, where capsids acquire the proteinaceous tegument layer and enveloping membrane. This involves budding into host membranes and subsequent exocytosis of assembled virions by fusion with the plasma membrane (3). Envelopment and exocytosis are thought to be mediated by small vesicles, leading to the continuous release of individually wrapped virions. However, groups of enveloped virus particles are also found inside multivesicular bodies (MVBs) (4, 5). Whether enveloped particles in MVBs reflect a productive envelopment and egress pathway or are targeted for lysosomal degradation has remained unknown.
Using a novel correlative light and electron microscopy (CLEM) workflow that enables imaging of virus morphogenesis in whole cells, we present evidence that HCMV envelopment does occur at MVBs, generating large intracellular accumulations of enveloped virions in HFF cells. Virus-filled MVBs carried exosomal markers and were found to traverse the cytoplasm to the plasma membrane by volumetric, live-cell lattice light-sheet microscopy. Using a pH-sensitive biosensor, we show that virus particles were released in bulk by fusion of MVBs with the plasma membrane leading to ‘patches’ of particles on the plasma membrane.
This hitherto undescribed envelopment and exocytosis pathway of HCMV, leading to the recurrent bulk release of virus particles, possibly involves the late-endosome/exosome pathway.

Significance Statement

HCMV is able to cause disease affecting various organs. Understanding how HCMV can infect a wide variety of cells is essential for developing antiviral strategies. Recent work suggests that HCMV particles with varying glycoprotein repertoires facilitate entry into different target cells. How this glycoprotein diversity at the single-particle-level is generated is unclear. Different envelopment and egress pathways might play a role.
Here, using HFF cells, we present direct functional evidence that HCMV uses multivesicular bodies for the bulk release of virus particles into membrane-associated accumulations as a novel, alternative HCMV egress pathway. Future work will aim to illuminate how different egress pathways might lead to varying virion compositions.

Main Text

Introduction

Human Cytomegalovirus (HCMV) is a highly prevalent herpesvirus that establishes lifelong latent infection in humans. It is the leading cause of congenital disabilities in the developed world and a significant cause of disease in immunocompromised patients, such a transplant, AIDS, or cancer patients (reviewed in (1)).
HCMV has the largest genome of all human herpesviruses, has a sophisticated lifecycle, and forms complex viral particles that contain numerous viral and host factors. Herpesvirus virions are assembled in a cumulating step called secondary envelopment. During secondary envelopment,

capsids associate with tegument proteins and bud into viral glycoprotein-containing membranes. After membrane scission, enveloped virus particles are contained inside vesicles. It has been shown for alphaherpesviruses that exocytic vesicles release individual enveloped virions at the plasma membrane by fusion (6). Compared to most alphaherpesviruses like the extensively studied Herpes Simplex Virus 1 (HSV-1), HCMV morphogenesis is much slower, taking not hours but several days. During this time, the virus extensively remodels the host cell's secretory apparatus leading to the formation of the assembly compartment (AC) (7). The AC is defined as a dense spherical, perinuclear structure consisting of convoluted and interconnected membranes. It displays many organelle-specific markers, including Golgi, trans-Golgi, endosomal, and lysosomal markers (4, 8–10) and is centered around the microtubule-organizing center (11). Current data suggest that HCMV capsids undergo secondary envelopment in the AC, but it is unclear which membranes are targeted. Proteomics indicate that the secretory apparatus's reorganization mixes membranes from different origins as targets for secondary envelopment (12, 13). Some EM-studies suggest that secondary envelopment events mostly happen individually at relatively small vesicles (14), while other studies found enveloped particles in large multivesicular bodies (MVBs) of unknown origin (4, 15–17). Deleting the viral protein pUL135 leads to an abrogation of MVB formation, and mutating pUL71 leads to a modulation of envelopment at MVBs, suggesting that HCMV actively influences MVB formation and targets MVBs for secondary envelopment (5, 16–19). A study in the related human herpesvirus 6A (HHV-6A) describes that it uses MVBs for an exosomal release pathway (20).

MVBs are believed to produce bulk pulses of extracellular vesicles (EVs) or exosomes by fusing with the plasma membrane (21–23). EVs can be produced by inward budding at late endosomes, which generates MVBs characterized by the presence of the late endosomal markers CD63, LAMP1, LAMP2, Rab4, and Rab5 (reviewed in (23)).

One mechanism described for the formation of MVBs is the endosomal sorting complex for transport (ESCRT) pathway (23). While parts of the ESCRT machinery play a role in the secondary envelopment of alphaherpesviruses (24–27), they likely do not in HCMV (28–30). Furthermore, it has lately been shown that HSV-1 proteins pUL7 and pUL51 form a complex that might constitute a mimic of an ESCRT-III complex. HCMV homologs pUL103 and pUL71 are structurally very similar to their HSV-1 counterparts and might likewise perform ESCRT functions for the virus during infection (27).

Moreover, molecules of the tetraspanin family, such as CD9, CD81, and CD63, have been described to be enriched on EV membranes (21). Tetraspanins are known to form microdomains called tetraspanin-enriched microdomains on the cell surface (31) and are active in the organization of the plasma membrane, recycling, and cellular signaling (31, 32). Importantly, tetraspanins are involved in sorting and targeting cargo to MVBs and, in cooperation with the ESCRT machinery, into EVs (33, 34). While it has been shown that HCMV-infected cells release EVs that contain viral surface proteins such as gB (35), the role of exosomal pathways in HCMV particle envelopment and release are largely not defined. Although Inhibitors of exosome biogenesis can slow HCMV spread, they do not seem to have a significant influence on viral titers (36, 37), possibly arguing for an involvement of the MVB/exosome-pathways in cell-to-cell spread. Interestingly, the authors did not find a significant effect of siRNA-mediated knockdown of CD63 on HCMV titers (37). At the same time, another very recent study shows a substantial reduction of HCMV titers upon CD63 siRNA knock-down, indicating that CD63 is indeed necessary for the production of infectious progeny (38). Moreover, in a very recent proteomics study, it was found that the host exosome pathway plays a role in HCMV assembly and egress. According to their data, HCMV utilizes parts of the exosome biogenesis machinery, such as VAMP3, independently of classical ESCRT-pathways (13).

In this study, we employed three-dimensional correlative light and electron microscopy (3D-CLEM) to investigate HCMV secondary envelopment and egress at the spatiotemporal level to elucidate whether HCMV indeed uses MVBs for egress. We found MVBs filled with virus particles and large viral accumulations between the cell and the growth substrate. Virus-containing MVBs carried markers of the exosomal pathway. Using live-cell confocal and volumetric lattice light-sheet

microscopy, we found that viral accumulations at the plasma membrane originated from intermittent pulses of fusing large intracellular bodies. Live-cell total internal reflection fluorescence (TIRF) microscopy confirmed that virus-filled MVBs are positive for the exosome/late endosome marker CD63 and were fusing with the plasma membrane, leading to pulses of local virus release and VEA formation.

Results

HCMV particles bud into and accumulate in MVBs

To analyze HCMV secondary envelopment and egress in 3D, we initially used volumetric spinning disk fluorescence microscopy and followed the fate of capsids and viral membranes with an HCMV mutant expressing EGFP-labeled capsid-associated tegument protein pp150 and mCherry-labeled glycoprotein gM (HCMV-TB40-UL32EGFP-UL100mCherry) (39). 4 days post-infection (dpi) we found two striking phenotypes in HFF cells: Large intracellular bodies positive for both markers (Fig. 1A-C) as well as patches of signal below the assembly compartment (Fig. 2A).
To uncover the nature of these structures, we developed a novel three-dimensional correlative light and electron microscopy (3D-CLEM) workflow that combines spinning disk fluorescence microscopy with serial block-face scanning electron microscopy (SBF-SEM). Indeed, 3D-CLEM (Fig 1B-C, Sup. Vid. 1A-B) confirmed that the intracellular bodies were vesicles filled with significant numbers of virions, dense bodies, as well as other structures (Fig 1C) previously described to be MVBs (5, 16), while the patches resolved to be accumulations of virus particles and other structures that resembled the content of these virus-filled MVBs (Fig. 2B, 2C, Sup. Vid. 2). In the following, we will call them viral extracellular accumulations (VEAs).
Virus-filled MVBs were very heterogeneous in size and content. Some contained only a few, others up to several hundred particles. Smaller vesicles were not as obvious in fluorescence microscopy (Fig 1C, 1D). Cells infected with wild-type HCMV showed a similar phenotype (Sup. Fig. 1).
Importantly, we found non-enveloped particles budding into MVBs, indicating that the MVBs were a target for de novo HCMV secondary envelopment, and the containing virus particles were virus progeny and not targeted for degradation (Figure 1D). Further, we observed large invaginations at the plasma membrane that harbored content similar to that found in MVBs, possibly indicating that MVBs released their content by fusion at the plasma membrane (Fig. 2C, Sup. Vid. 2).

Intermittent bulk release leads to viral extracellular accumulations at the plasma membrane

To understand how VEAs are formed at the plasma membrane, we performed time-lapse live-cell fluorescence microscopy experiments. First, we utilized inverted lattice light-sheet microscopy to acquire time-lapse volumes at high temporal resolution for 15-45 minutes with minimal phototoxicity and photobleaching. We found that large bodies, possibly resembling MVBs, traveled from the assembly complex to the plasma membrane with subsequent formation of a VEA (Figure 3A, Sup. Vid. 3). In a second approach, we investigated longer timespans in the infection cycle to investigate if this mechanism is a possible general mechanism for accumulation at the plasma membrane in HCMV infection. Here we used a modified HCMV mutant, with more photostable fluorescent tags (HCMV-TB40-UL32SNAP-UL100mScarlet-I), for imaging z-stacks over several days. We imaged HFF cells that had not yet produced extracellular accumulation between 72 and 96 hpi for 18 to 60 hours every 40 minutes with a spinning-disc-confocal fluorescence microscope. Strikingly, we found that VEA formation generally occurred as intermittent pulses of vesicles coming into the observation plane near the plasma membrane and seemingly relaxing into VEAs (Figure 3B, Sup. Vid. 4-5). Release events varied in fluorescence intensity, which is consistent with our observation that MVBs were very heterogeneous in size.

Virus-containing MVBs carry markers of the endocytic trafficking system and the exosome pathway

Intermittent bulk release of vesicles is a hallmark of exosomal pathways. Therefore, we applied an immunofluorescence methodology combined with mass spectrometry based proteomics to uncover possible overlaps between virus composition and exosome generation. To this end, we performed mass spectrometry analysis of gradient-purified extracellular virions. Gradient-purified virus particles contained markers of Golgi-to-endosome trafficking (syntaxin 12, rab14, VAMP3), early endosomes (Rab 5C, syntaxin 7), as well as exosomes (HSP70, HSP90, GAPDH, enolase 1, 14-3-3 and PKM2), suggesting that HCMV might use a fusion of Golgi- and endosomal membranes for secondary envelopment to generate virus-filled MVBs (Sup. Table 1). These findings are consistent with a recent publication from Turner et al., in which proteomics was used to analyze commonalities between host exosome pathways and HCMV infection products. Our results also confirm this publication, concluding that the exosome pathway is significantly involved in facilitating HCMV egress (13).
Other classical markers for membranes used in the exosomal pathway are the tetraspanins CD9, CD63, and CD81. CD63 has been investigated in the context of HCMV infection before, however, with conflicting results (37, 38). Using immunofluorescence, we tested if they might be localized to virus filled MVBs. We found CD63 localizing to large vesicles also containing pp150 and gM (Fig. 4 A-C) while CD9 and CD81 localized to the AC but not specifically to MVBs (Fig S2A, S2B). Exocytosed particles in VEAs did not show any CD63, implying that CD63 is unlikely to be incorporated into virions. This observation is supported by the absence of CD63 in virion proteomic data (Sup. Tab. 1) (40).

HCMV-containing MVBs release their cargo through fusion with the plasma membrane

To confirm that the observed bulk release events were indeed fusion events with the plasma membrane, we created a cell line stably producing a CD63-pHluorin fusion construct developed by the Pegtel Lab (41). In this construct, the pH-sensitive fluorescent protein pHluorin is inserted into an extracellular loop of CD63, such that it points towards the luminal side in vesicles and to the extracellular environment after fusion. Through this approach, the super-ecliptic-pHluorin is quenched by the acidic pH inside this luminal space, rendering the construct non-fluorescent. However, upon fusion with the plasma membrane, the pHluorin gets exposed to the pH-neutral extracellular milieu, and the fluorescence recovers rapidly. The increase in fluorescence activity provides an easily detectable indicator of MVB fusion. Imaging of fixed cells confirmed that the fluorescence signal from the CD63-fusion localized to large gM and gB positive bodies, indicating that CD63 might be involved in viral progeny production (Fig 4A).
For imaging of potential fusion events, we picked cells that had not yet accumulated VEAs on the outside of the basolateral cell surface and used live-cell total internal reflection microscopy (TIRF) to image fusion events for several hours without phototoxicity. We took images every 1.5-2 seconds for 60 minutes since we predicted that actual membrane fusion and pH equilibration might be very rapid. We found that large MVBs came into the TIRF-field and relaxed into VEAs shortly after arrival at the plasma membrane. Strikingly, flashes in green fluorescence between the large round body's arrival and the relaxation event occurred, indicating that membranes had fused. The short flashes of green fluorescence are indicative of most CD63 quickly diffusing away from the fusion site (Figure 5A-B). The transition from round MVBs to VEAs took much longer than the actual fusion event, suggesting that fusion pore expansion and cargo expulsion are slow, possibly explaining the frequent appearance of particle-filled invaginations in SBF-SEM images.

Discussion

Little data exist on the spatiotemporal organization of HCMV egress at the subcellular level. Studies using transmission EM have shown that virus-filled MVBs can form in HCMV-infected cells and HHV-6A and MCMV infected cells (4, 5, 16, 20, 42). However, a functional role for MVBs in egress has lacked so far (4, 15–17). Here we report that HCMV can form virus particles by budding into MVBs using a novel 3D-CLEM workflow that combines dynamic information from spinning disk

fluorescence microscopy with high spatial information from serial block-face scanning electron microscopy. Using time-lapse and functional live cell imaging, we provide data suggesting that virus filled MVBs can fuse with the plasma membrane and release tens to hundreds of virus particles in bulk, resulting in plasma membrane-associated VEAs. Finally, proteomics of purified virions, functional imaging, and correlation of CD63 with MVBs suggest that MVB-mediated HCMV egress might be connected to an exosomal pathway.

While virus-filled MVBs have been described in HCMV-infected cells, it was unclear if these were part of a productive egress pathway. Previous studies have mostly reported single-virion/single-vesicle envelopment events, which have shaped our current picture of HCMV secondary envelopment (14, 16). Live-cell imaging indicates that virus-filled MVBs form relatively quickly between 72 and 96 hpi and are soon released asynchronously. Our new correlative SBF-SEM workflow permits us to focus on these transient events by preselecting cells using specific markers in light microscopy. Moreover, the much higher throughput of block-face-cutting compared to precise but tedious serial sectioning (14) might have allowed us to get a better overview of the infection phenotype.

Our data is in line with previous work that suggests that Golgi- and endosome-derived membranes are targeted for secondary envelopment and might result in virus-filled MVBs (4, 8–10, 15, 40). We found colocalization between the tetraspanin CD63 and gB, gM, and pp150. However, CD81 and CD9, which are also associated with exosomes, did not colocalize with the viral markers as strongly. Since VEAs were negative for CD63, this marker might be excluded during the budding process at the MVB surface. CD63 possibly plays a role in the sorting of viral glycoproteins to sites of secondary envelopment, as tetraspanins are known to be involved in sorting plasma membrane-bound molecules into MVBs (33, 34). HCMV gB is known to localize to the plasma membrane and be sorted through endocytic and recycling pathways by an acidic cluster in its cytoplasmic domain. (Radsak213:1996, Tugizov3h:1999) For HSV-1, it was reported that disrupting the endosome-to-MVB trafficking pathway leads to mislocalization of the HSV-1 gB (43). More recently, it has also been reported that HSV-1 replication leads to an increase of exocytosis of CD63 with extracellular vesicles, leading the authors to hypothesize that HSV-1 modulates exosome biogenesis for its benefit (44). Taken together, these reports indicate that endocytic pathways can be involved in the trafficking of viral factors to sites of Herpesvirus secondary envelopment. Our observation that HCMV gB strongly localized with CD63 might support this hypothesis and fits a recent report that gB is enriched in exosomes (35). A very recent preprint also argues that virus-filled MVBs in fibroblasts are derived from the canonical endocytic pathway and hijack the classical exosomal pathway (45). Moreover, a recent proteomics study focusing on exosome release from HCMV infected cells is in line with this interpretation (13). This study was further able to identify several further viral proteins that likewise appear in exosomes. The data provided by the authors further strengthen the overall idea that HCMV exploits endocytic trafficking and exosome biogenesis pathways for the assembly and egress of virus particles.

MVB-mediated egress might be an alternative pathway to using small vesicles as it was reported for the alphaherpesvirus PRV and was implied for HCMV (6, 14). HCMV predominantly produces cell-associated progeny in endothelial cells. In contrast, fibroblasts produce large amounts of cell-free virus in addition to cell-associated virus (46). These different populations vary in their glycoprotein composition and cell tropism, and it is plausible to hypothesize that these virus populations might undergo different envelopment processes in the cell and are exocytosed with a different spatiotemporal profile (46).

The VEAs that we observed were largely static during live-cell imaging and might represent a cell-associated viral population. However, 3D-EM showed that most particles were not directly associated with the membrane but were trapped between the cell and the cell support. Moreover, purified virions showed markers of the exosome pathway, and it is unlikely that cell-associated virus was co-purified (13).

Alternatively to budding, virus-filled MVBs might result from individual virus-filled transport vesicles fusing as suggested for HHV-6A (20). This idea fits to reports that MVBs were mostly found in the AC periphery while most capsid budding into individual vesicles is observed in the center of the AC, where early endosomal markers and Golgi-markers merge (8, 9). However, in this study, we regularly found budding events at MVBs but could not identify fusion events in full 3D-EM volumes.

In summary, we provide evidence for a novel functional egress pathway of HCMV in fibroblasts using a novel correlative 3D-EM workflow and functional light microscopy that indicates that HCMV buds into early endosome-derived membranes to generate MVBs, which subsequently fuse with the plasma membrane intermittently to release virus particles into membrane-associated VEAs in bulk. Future work is needed to delineate the molecular mechanism involved as well as its biological role. This includes verifying whether factors or mechanisms from exosome pathways are functionally involved in viral morphogenesis or if they show up as bystanders in our assays. Furthermore, we do not know yet whether HCMV egress occurs at specialized egress sites as it is discussed for the alphaherpesviruses PRV and HSV-1 (6, 47). Also, the question if the HCMV particles, which are released through one or the other pathway, are equally infectious remains unanswered at this point. However, the model of different egress pathways might raise important questions and give valuable cues for research investigating HCMV spread in different viral strains, cell types, and tissues, which was argued for very recently (45).

Materials and Methods

Cells and Viruses

HFF-1 cells were acquired from ATCC (ATCC-SCRC-1041) and cultivated in Dulbecco's Modified Eagles Medium Glutamax Dulbecco's Modified Eagles Medium Glutamax (Thermofisher) supplemented with 5% FBS superior (Merck) and $2*10^5$ units/ml Recombinant Human FGF-basic (Pepro Tech). HCMV-UL32EGFP-UL100mCherry was a kind gift by Christian Sinzger (39). The HCMV-TB-40-BAC4 was a kind gift by Wolfram Brune (48).

Spinning Disk Fluorescence Microscopy

Spinning disk microscopy was carried out on a Nikon TI2 based spinning disk system equipped with a Yokogawa W2, a Nikon 1.49 NA Apo-TIRF objective, and an Andor iXON888 EMCCD. The resulting pixel size was 130nm, and image acquisition was done with NIS-Elements. Further, the setup was equipped with 405, 488, 561, and 640 laser lines and corresponding filter sets. Life cell experiments were carried out with a humidified incubation chamber heated to 37°C and 5% CO2 controlled by a gas-mixer. For fluorescence microscopy, cells were grown in Ibidi 35mm glass-bottom dishes, for CLEM in Ibidi 35mm grid polymer bottom dishes. SNAP labeling before live-cell imaging with SNAP-Cell 647-SIR (NEB) was done as described in the manual from the manufacturer. Image processing and analysis were performed in ImageJ/FIJI.

Serial Block Face Scanning Electron Microscopy (SBF-SEM)

For SBF-SEM, cells were fixed at the indicated time-points with 2% Paraformaldehyde (PFA/ Science Services) and 2.5% Glutaraldehyde (GA/ Science Services) in Dulbecco's phosphate-buffered saline (D-PBS, Sigma-Aldrich) for 5 minutes at room temperature (RT) and 55 minutes on ice. Subsequently, the sample was processed with the following procedure: Postfixation with 2% Osmium Tetroxide (OsO_4/ Science Services) and 2.5% GA in D-PBS on ice, staining with 2% OsO_4, 1.5% potassium ferrocyanide (Sigma), 2mM $CaCl_2$ (Sigma) in water, incubation in 0.5% thiocarbohydrazide (Sigma) in water, staining with 2% OsO_4 in water, incubation in 1% gallic acid (Sigma) in water, staining with 2% uranyl acetate (Merck) overnight in water. On the next day, the sample was stained with freshly prepared Waltons lead aspartate (49) ($Pb(NO_3)_2$ (Roth), L-Aspartate (Roth), KOH (Merck)), and subsequently subjected to a PLT dehydration series to

Ethanol Rotipuran (Roth). Finally, the samples were infiltrated with 70% Epon in Ethanol before two incubations with 100% Epon and the final polymerization was carried out in Epon supplemented with 3% silver flakes (Sigma) and 3% (w/w) Ketjen Black (TAAB). Sample blocks of 0.5x0.5 mm were cut, mounted, and inserted into a Gatan 3view stage built in a Jeol X scanning electron microscope. For imaging, the sample stage was biased with a 500V positive charge to account for sample charging during the scanning process. For the acquisition, 3x3 nm pixel size images were scanned, followed by the repeated ablation of 50 nm sections. The acquisition was controlled by the Gatan Digital Micrograph software, which was also used for stack alignments. Further processing of the datasets was performed in FIJI, and the volumes were rendered in Imaris 8.

Transmission Electron Microscopy (TEM)

For TEM, cells were fixed and processed as described for SBF-SEM up to the embedding step. The cells were embedded in Epon without fillers, sectioned to 50 nm on a Leica Ultracut Microtome (Leica), and subsequently transferred to copper mesh grids. Electron microscopy was performed on an FEI Tecnai G20 (FEI/Thermofisher).

Lattice Light Sheet Microscopy

Lattice light-sheet microscopy was performed on a Zeiss Lattice Light Sheet 7 (Zeiss) as part of an early adaptor program, controlled with Zeiss Zen Blue software. The device is equipped with 488, 561, and 640 laser lines and multi-bandpass filters. Live-cell experiments were carried out on Ibidi 35mm glass-bottom dishes at 37°C with 5% CO2 in a humidified atmosphere. The acquisition was done on a pco.edge (PCO) sCMOS camera with a final pixel size of 145nm. Images were deconvolved after acquisition in Zen Blue using the built-in constrained-iterative algorithm. 2D image processing was done in Zen Blue, arrangements and montages were done in FIJI. 3D image processing was done in Arivis 4D; videos were cut and arranged in Adobe Premiere Pro.

BAC Mutagenesis

BAC mutagenesis was performed as described before by en-passant Red Recombination (50). The creation of HCMV-TB40/BAC4-UL32SNAP-UL100mScarlet-I was done in two steps. At first, UL32 was mutated by the C-terminal insertion (after K1045) of the SNAP-Tag-SCE-I-KanR shuttle sequence with a nine amino acid linker (HTEDPPVAT) and subsequent second recombination to clear the Kanamycin resistance and restore the SNAP-Tag sequence (complete insertion sequence see Table 1/ REF SNAP-Tag). This was followed up by the insertion of the mScarlet-I sequence between amino acids V62 and M63 of gM by amplifying the mScarlet-I-SCE-I-KanR shuttle construct with the primers shown in Table 2, with the second recombination as described for the first step. The virus was reconstituted by electroporation of the BAC DNA into HFF cells.

Gateway Cloning and Lentivirus Transduction

Plasmid pCMV-Sport6-CD63pHluorin was a gift from DM Pegtel (Addgene plasmid # 130601 ; http://n2t.net/addgene:130901 ; RRID:Addgene_130901). For Gateway (Thermofisher) cloning, the pCMV-Sport6-CD63pHluorin was recombined with pDONR-221 (Thermofisher) to produce the pENTR-CD63pHluorin vector that was further recombined with pLenti-CMV-Puro-DEST (w118-1), a gift from Eric Campeau & Paul Kaufman (Addgene plasmid # 17452; http://n2t.net/addgene:17452; RRID: Addgene_17452).
The resulting pLenti-CMV-CD63pHluorin-Puro was then transfected with polyethyleneimine (Polysciences) together with 3rd generation Lentivirus vector helper plasmids, gifts by Didier Trono, RRID: Addgene_12253, Addgene_12251, Addgene_12259) into 293XT cells (Takara). Lentivirus containing supernatant was harvested at 48, 72, and 96 hours post transfection, filtered through 0.2 µm syringe filters, and used to transduce HFF-1 cells. 72hpi, the HFF-cells were selected with

Puromycin at 5 µg/ml. Furthermore, the cells were sorted by fluorescence-activation (FACS), using a FACS Aria Fusion (BD Biosciences), for the 10% strongest fluorescent cells, further cultivated and used for the experiments.

Immunofluorescence

For immunofluorescence experiments, cells were grown in 35mm glass-bottom Ibidi dishes and fixed at the indicated time-points with 4%PFA in D-PBS. SNAP labeling with SNAP-Cell 647-SIR was done as described in the manual for SNAP-Cell 647-SIR (NEB). Afterwards, the samples were permeabilized with TritonX-100 at 0.1% in D-PBS with subsequent blocking with 3% Bovine Serum Albumin (Sigma) in D-PBS. Primary antibodies used in this study were Ultra-LEAF™ Purified anti-human CD63 H5C6 (Biolegend), Anti-Cytomegalovirus Glycoprotein B antibody [2F12] (ab6499) (Abcam), Purified anti-human CD9 HI9a (Biolegend), Purified anti-human CD81 (TAPA-1) 5A6 (Biolegend). Secondary antibodies used were Alexa 647 goat anti-mouse (Thermofisher) and Alexa 488 goat anti-mouse (Thermofisher).

Confocal Scanning Imaging

Confocal Laser Scanning Microscopy was carried out on a Nikon TI2 microscope equipped with an A1 confocal laser scanning unit, a 1.4 NA 60x Plan Apo objective, PMT, and GaAsP detectors, standard 404, 489, 561, and 637 laser lines, and corresponding filter sets. Imaging conditions were optimized for each sample. Scan sizes were adapted to fulfill the criteria for Nyquist-sampling, resulting in a pixel size of 118 nm. The acquisition was done in NIS-Elements, post-processing and image analysis were performed in FIJI.

Weighted Spatial Colocalization Analysis

For the weighted colocalization heatmaps, pixel intensities were calculated, taking into account the absolute intensities in both channels, as well as the ratio between the intensities. The calculation was performed by first normalizing each channel to relative intensity. In the following, the relative intensities of each pixel in both channels a and b were interpreted as a vector$\binom{a}{b}$, describing the vector to the position of that pixel in a classical scatter plot. The length of the vector was then multiplied by $1 - |\sin(\alpha) - \cos(\alpha)|$ while α being the angle between the vector and the x-axis. This multiplication emphasizes pixels where the two colors colocalize with similar relative intensities. The product then was plotted back to the original pixel position in the image resulting in the heatmap shown in the figures. With this strategy, we could put the information of a 2-channel scatter plot back into the image's spatial context.

Gradient purification of HCMV

A 15 cm dish of HFF cells was infected with HCMV-TB40-WT at MOI 0.05. Seven dpi, the infected cells were trypsinized and split onto 16x 15 cm dishes of HFF cells. At 7 dpi, the supernatant was harvested and clarified by centrifugation at 1200 xg for 5 min. The virus was pelleted by centrifugation at 14000xg for 1.5 h at 4°C and then resuspended in 1% FBS/PBS overnight on ice. The resuspended virus was centrifuged at 18000xg for 1 min at 4°C to remove large aggregates and then loaded over a continuous gradient made from 15% sodium tartrate with 30% glycerol (w/w) and 35% sodium tartrate (w/w) in 40 mM sodium phosphate pH 7.4 (51). The gradient was made with a Gradient Master (BioComp Instruments) for an SW41 rotor. After centrifugation at 65000xg for 1.5 h at 4°C, the bands were isolated, diluted 10-fold in PBS, and pelleted at 14000xg for 1.5 h at 4°C. The purified virus pellet was resuspended overnight in PBS and then stored at -80°C.

Mass Spectrometry

The purified virus was mixed with 3 volumes of lysis buffer (100 mM Tris, 50 mM DTT, 8 M Urea pH 8.5) and incubated at room temperature for 15 min. Samples were digested using the FASP protocol, employing 30 kDa molecular weight cut-off filter centrifugal units (Amicon, (52)). Briefly, lysed virus was added to the centrifugal unit and washed with TU buffer (100 mM Tris, 8 M Urea pH 8.5). Next, 8 mM DTT in TU buffer was added and incubated at 56°C for 15 min. After two further washes, 50 mM iodoacetamide (IAA) in TU buffer was added and incubated for 10 minutes at room temperature. The centrifugal units were washed twice, treated again with DTT, washed once further with TU buffer and twice with 50 mM ammonium bicarbonate solution. MS grade trypsin (Promega) was added in a 1:100 enzyme:protein ratio and the sample incubated overnight at 37°C. The flow-through containing trypsinized peptides was collected and pooled, and the sample lyophilized with a SpeedVac (Thermo). The resulting peptides were enriched with C18 stage tips prepared in house and eluted with 80% acetonitrile containing 0.5% acetic acid. The samples were dried down by SpeedVac (Thermo) and resuspended in 97% water, 3% acetonitrile with 0.1% formic acid, and 10 fmol/µL E. coli digest (Waters Corporation) for analysis by LC-MS/MS.

Peptides resulting from trypsinization were analyzed on a Synapt G2-Si QToF mass spectrometer connected to a NanoAcquity Ultra Performance UPLC system (both Waters Corporation). The data acquisition mode used was mobility enhanced MSE over m/z range 50-2000 with the high energy collisional voltage in the transfer region ramped from 25 to 55 V. Mobile phases used for chromatographic separation were water with 0.1% formic acid (A) and acetonitrile with 0.1% formic acid (B). Samples were desalted using a reverse-phase SYMMETRY C18 trap column (100 Å, 5 µm, 180 µm x 20 mm, Waters Corporation) at a flow rate of 8 µl/min for 2 minutes. Peptides were separated by a linear gradient (0.3 µl/min, 35 °C; 97-60% mobile phase A over 90 minutes) using an Acquity UPLC M-Class Reversed-Phase (1.7 µm Spherical Hybrid, 76 µm x 250 mm, Waters Corporation).

LC-MS data were peak detected and aligned by Progenesis QI for proteomics (Waters Corporation). Proteins were identified by searching against the Human and HCMV proteomes in Uniprot. The database search was performed with the following parameters: mass tolerance was set to software automatic values; enzyme specified as trypsin; up to two missed cleavages; cysteine carbamidomethylation as a fixed modification, with the oxidation of methionine, S/T phosphorylation, and N-terminal acetylation set as variable modifications. Abundances were estimated by Hi3-based quantitation (53).
For comparison with the Turner et al., dataset protein accession was converted to UniParc codes. Raw MS data have been deposited to PRIDE with accession code XXXX. (Accession Code will be provided as soon as the data is successfully deposited)

Live TIRF Microscopy

For live-cell TIRF imaging, infection experiments were carried out in 35 mm glass-bottom Ibidi dishes. SNAP labeling with SNAP-Cell 647-SIR was done as described in the manual for SNAP-Cell 647-SIR (NEB) before imaging. Microscopy was performed on a Nikon TI equipped for TIRF microscopy and equipped with standard 488, 561, and 640 laser lines, corresponding filter sets, and an incubation chamber with a heating system. The illumination angle was determined experimentally by manually adjusting for TIRF illumination, and image acquisition was performed with NIS-Elements using an ANDOR iXon Ultra 897 EMCCD camera. Live-cell experiments were carried out at 37°C. Intensity measurements in the time courses were done with FIJI by the manual placing of ROIs. Analysis of the data and visualization in the graphs was performed in GraphPad Prism.

Acknowledgments

We thank Wolfram Brune, Christian Sinzger, and Kerstin Sampaio for their generous gift of viruses HCMV-TB-40-BAC4 HCMV-UL32EGFP-UL100mCherry and their support.

This study was funded by the Wellcome Trust through a Collaborative Award (209250/Z/17/Z) to KT, KG, and JBB. KG and JBB are funded by the Deutsche Forschungsgemeinschaft (DFG, German Research Foundation) under Germany's Excellence Strategy – EXC 2155 – project number 390874280. We thank the DFG for funding the lattice light sheet system through a large equipment grant to KG and JB, project number 413831413. We thank Zeiss for including us in their lattice light-sheet early adaptor program. FF is holding a graduate student fellowship by the Studienstiftung des deutschen Volkes. The Heinrich Pette Institute, Leibniz Institute for Experimental Virology is supported by the Free and Hanseatic City of Hamburg and the Federal Ministry of Health. This study is part of the Leibniz ScienceCampus InterACt (Grant Agreement No. W6/2018). The mass spectrometer used in this study was funded by a Wellcome Trust grant 104913/Z/14/Z

References

1. P. Griffiths, The direct and indirect consequences of cytomegalovirus infection and potential benefits of vaccination. *Antivir Res* **176**, 104732 (2020).
2. J. C. Alwine, The Human Cytomegalovirus Assembly Compartment: A Masterpiece of Viral Manipulation of Cellular Processes That Facilitates Assembly and Egress. *Plos Pathog* **8**, e1002878 (2012).
3. T. C. Mettenleiter, Herpesvirus Assembly and Egress. *J Virol* **76**, 1537–1547 (2002).
4. M. Homman-Loudiyi, K. Hultenby, W. Britt, C. Söderberg-Nauclér, Envelopment of Human Cytomegalovirus Occurs by Budding into Golgi-Derived Vacuole Compartments Positive for gB, Rab 3, Trans-Golgi Network 46, and Mannosidase II. *J Virol* **77**, 3191–3203 (2003).
5. F. Bughio, D. A. Elliott, F. Goodrum, An Endothelial Cell-Specific Requirement for the UL133-UL138 Locus of Human Cytomegalovirus for Efficient Virus Maturation. *J Virol* **87**, 3062–3075 (2013).
6. I. B. Hogue, J. B. Bosse, J.-R. Hu, S. Y. Thiberge, L. W. Enquist, Cellular Mechanisms of Alpha Herpesvirus Egress: Live Cell Fluorescence Microscopy of Pseudorabies Virus Exocytosis. *Plos Pathog* **10**, e1004535 (2014).
7. V. Sanchez, K. D. Greis, E. Sztul, W. J. Britt, Accumulation of Virion Tegument and Envelope Proteins in a Stable Cytoplasmic Compartment during Human Cytomegalovirus Replication: Characterization of a Potential Site of Virus Assembly. *J Virol* **74**, 975–986 (2000).
8. S. Das, A. Vasanji, P. E. Pellett, Three-Dimensional Structure of the Human Cytomegalovirus Cytoplasmic Virion Assembly Complex Includes a Reoriented Secretory Apparatus ▿ †. *J Virol* **81**, 11861–11869 (2007).
9. S. Das, P. E. Pellett, Spatial Relationships between Markers for Secretory and Endosomal Machinery in Human Cytomegalovirus-Infected Cells versus Those in Uninfected Cells. *J Virol* **85**, 5864–5879 (2011).
10. V. Cepeda, M. Esteban, A. Fraile- Ramos, Human cytomegalovirus final envelopment on membranes containing both trans- Golgi network and endosomal markers. *Cell Microbiol* **12**, 386–404 (2010).
11. D. J. Procter, *et al.*, The HCMV Assembly Compartment Is a Dynamic Golgi-Derived MTOC that Controls Nuclear Rotation and Virus Spread. *Dev Cell* **45**, 83-100.e7 (2018).
12. N. J. Moorman, R. Sharon-Friling, T. Shenk, I. M. Cristea, A Targeted Spatial-Temporal Proteomics Approach Implicates Multiple Cellular Trafficking Pathways in Human Cytomegalovirus Virion Maturation. *Mol Cell Proteomics* **9**, 851–860 (2010).
13. D. L. Turner, D. V. Korneev, J. G. Purdy, A. de Marco, R. A. Mathias, The host exosome pathway underpins biogenesis of the human cytomegalovirus virion. *Elife* **9**, e58288 (2020).

14. M. Schauflinger, C. Villinger, T. Mertens, P. Walther, J. Einem, Analysis of human cytomegalovirus secondary envelopment by advanced electron microscopy. *Cell Microbiol* **15**, 305–314 (2013).
15. J. Tooze, M. Hollinshead, B. Reis, K. Radsak, H. Kern, Progeny vaccinia and human cytomegalovirus particles utilize early endosomal cisternae for their envelopes. *Eur J Cell Biol* **60**, 163–78 (1993).
16. M. Schauflinger, *et al.*, The Tegument Protein UL71 of Human Cytomegalovirus Is Involved in Late Envelopment and Affects Multivesicular Bodies. *J Virol* **85**, 3821–3832 (2011).
17. F. Bughio, M. Umashankar, J. Wilson, F. Goodrum, Human Cytomegalovirus UL135 and UL136 Genes Are Required for Postentry Tropism in Endothelial Cells. *J Virol* **89**, 6536–6550 (2015).
18. C. S. Meissner, S. Suffner, M. Schauflinger, J. von Einem, E. Bogner, A Leucine Zipper Motif of a Tegument Protein Triggers Final Envelopment of Human Cytomegalovirus. *J Virol* **86**, 3370–3382 (2012).
19. A. N. Dietz, C. Villinger, S. Becker, M. Frick, J. von Einem, A Tyrosine-Based Trafficking Motif of the Tegument Protein pUL71 Is Crucial for Human Cytomegalovirus Secondary Envelopment. *J Virol* **92**, e00907-17 (2018).
20. Y. Mori, *et al.*, Human Herpesvirus- 6 Induces MVB Formation, and Virus Egress Occurs by an Exosomal Release Pathway. *Traffic* **9**, 1728–1742 (2008).
21. C. Théry, L. Zitvogel, S. Amigorena, Exosomes: composition, biogenesis and function. *Nat Rev Immunol* **2**, 569–579 (2002).
22. E. Cocucci, G. Racchetti, J. Meldolesi, Shedding microvesicles: artefacts no more. *Trends Cell Biol* **19**, 43–51 (2009).
23. M. Colombo, G. Raposo, C. Théry, Biogenesis, Secretion, and Intercellular Interactions of Exosomes and Other Extracellular Vesicles. *Annu Rev Cell Dev Bi* **30**, 1–35 (2014).
24. C. M. Crump, C. Yates, T. Minson, Herpes Simplex Virus Type 1 Cytoplasmic Envelopment Requires Functional Vps4 ▿. *J Virol* **81**, 7380–7387 (2007).
25. T. Pawliczek, C. M. Crump, Herpes Simplex Virus Type 1 Production Requires a Functional ESCRT-III Complex but Is Independent of TSG101 and ALIX Expression ▿. *J Virol* **83**, 11254–11264 (2009).
26. H. Kharkwal, C. G. Smith, D. W. Wilson, Blocking ESCRT-Mediated Envelopment Inhibits Microtubule-Dependent Trafficking of Alphaherpesviruses In Vitro. *J Virol* **88**, 14467–14478 (2014).
27. B. G. Butt, *et al.*, Insights into herpesvirus assembly from the structure of the pUL7:pUL51 complex. *Elife* **9**, e53789 (2020).
28. R. Tandon, D. P. AuCoin, E. S. Mocarski, Human Cytomegalovirus Exploits ESCRT Machinery in the Process of Virion Maturation ▿. *J Virol* **83**, 10797–10807 (2009).
29. A. Fraile- Ramos, *et al.*, The ESCRT machinery is not required for human cytomegalovirus envelopment. *Cell Microbiol* **9**, 2955–2967 (2007).
30. N. T. Streck, J. Carmichael, N. J. Buchkovich, Nonenvelopment Role for the ESCRT-III Complex during Human Cytomegalovirus Infection. *J Virol* **92**, e02096-17 (2018).
31. M. Yáñez-Mó, O. Barreiro, M. Gordon-Alonso, M. Sala-Valdés, F. Sánchez-Madrid, Tetraspanin-enriched microdomains: a functional unit in cell plasma membranes. *Trends Cell Biol* **19**, 434–446 (2009).
32. T. Takino, *et al.*, Tetraspanin CD63 promotes targeting and lysosomal proteolysis of membrane-type 1 matrix metalloproteinase. *Biochem Bioph Res Co* **304**, 160–166 (2003).
33. G. van Niel, *et al.*, The Tetraspanin CD63 Regulates ESCRT-Independent and -Dependent Endosomal Sorting during Melanogenesis. *Dev Cell* **21**, 708–721 (2011).
34. D. Perez-Hernandez, *et al.*, The Intracellular Interactome of Tetraspanin-enriched Microdomains Reveals Their Function as Sorting Machineries toward Exosomes. *J Biol Chem* **288**, 11649–11661 (2013).
35. S. Zicari, *et al.*, Human cytomegalovirus-infected cells release extracellular vesicles that carry viral surface proteins. *Virology* **524**, 97–105 (2018).

36. N. Kosaka, *et al.*, Secretory Mechanisms and Intercellular Transfer of MicroRNAs in Living Cells. *J Biol Chem* **285**, 17442–17452 (2010).
37. N. T. Streck, Y. Zhao, J. M. Sundstrom, N. J. Buchkovich, Human Cytomegalovirus Utilizes Extracellular Vesicles to Enhance Virus Spread. *J Virol* (2020) https:/doi.org/10.1128/jvi.00609-20.
38. Y. Hashimoto, X. Sheng, L. A. Murray-Nerger, I. M. Cristea, Temporal dynamics of protein complex formation and dissociation during human cytomegalovirus infection. *Nat Commun* **11**, 806 (2020).
39. K. Sampaio, G. Jahn, C. Sinzger, Virus-Host Interactions, Methods and Protocols. *Methods Mol Biology Clifton N J* **1064**, 201–209 (2013).
40. S. M. Varnum, *et al.*, Identification of Proteins in Human Cytomegalovirus (HCMV) Particles: the HCMV Proteome. *J Virol* **78**, 10960–10966 (2004).
41. M. P. Bebelman, *et al.*, Real-time imaging of multivesicular body–plasma membrane fusion to quantify exosome release from single cells. *Nat Protoc* **15**, 102–121 (2020).
42. S. Maninger, *et al.*, M94 Is Essential for the Secondary Envelopment of Murine Cytomegalovirus ‡. *J Virol* **85**, 9254–9267 (2011).
43. A. Calistri, *et al.*, Intracellular Trafficking and Maturation of Herpes Simplex Virus Type 1 gB and Virus Egress Require Functional Biogenesis of Multivesicular Bodies ▿. *J Virol* **81**, 11468–11478 (2007).
44. C. Dogrammatzis, T. Deschamps, M. Kalamvoki, Biogenesis of extracellular vesicles during herpes simplex virus type 1 infection: The role of the CD63 tetraspanin. *J Virol* **93**, JVI.01850-18 (2018).
45. S. Momtaz, B. Molina, L. Mlera, F. Goodrum, J. M. Wilson, Cell type-specific biogenesis of novel vesicles containing viral products in human cytomegalovirus infection. *Biorxiv*, 2020.12.10.420711 (2020).
46. L. Scrivano, C. Sinzger, H. Nitschko, U. H. Koszinowski, B. Adler, HCMV Spread and Cell Tropism are Determined by Distinct Virus Populations. *Plos Pathog* **7**, e1001256 (2011).
47. R. M. Mingo, J. Han, W. W. Newcomb, J. C. Brown, Replication of Herpes Simplex Virus: Egress of Progeny Virus at Specialized Cell Membrane Sites. *J Virol* **86**, 7084–7097 (2012).
48. C. Sinzger, *et al.*, Cloning and sequencing of a highly productive, endotheliotropic virus strain derived from human cytomegalovirus TB40/E. *J Gen Virol* **89**, 359–368 (2008).
49. J. Walton, Lead asparate, an en bloc contrast stain particularly useful for ultrastructural enzymology. *J Histochem Cytochem Official J Histochem Soc* **27**, 1337–1342 (1979).
50. B. K. Tischer, G. A. Smith, N. Osterrieder, In Vitro Mutagenesis Protocols, Third Edition. 421–430 (2010).
51. P. Talbot, J. D. Almeida, Human Cytomegalovirus: Purification of Enveloped Virions and Dense Bodies. *J Gen Virol* **36**, 345–349 (1977).
52. U. Distler, J. Kuharev, P. Navarro, S. Tenzer, Label-free quantification in ion mobility–enhanced data-independent acquisition proteomics. *Nat Protoc* **11**, 795–812 (2016).
53. J. C. Silva, M. V. Gorenstein, G.-Z. Li, J. P. C. Vissers, S. J. Geromanos, Absolute Quantification of Proteins by LCMSE A Virtue of Parallel ms Acquisition. *Mol Cell Proteomics* **5**, 144–156 (2006).

Figures and Tables

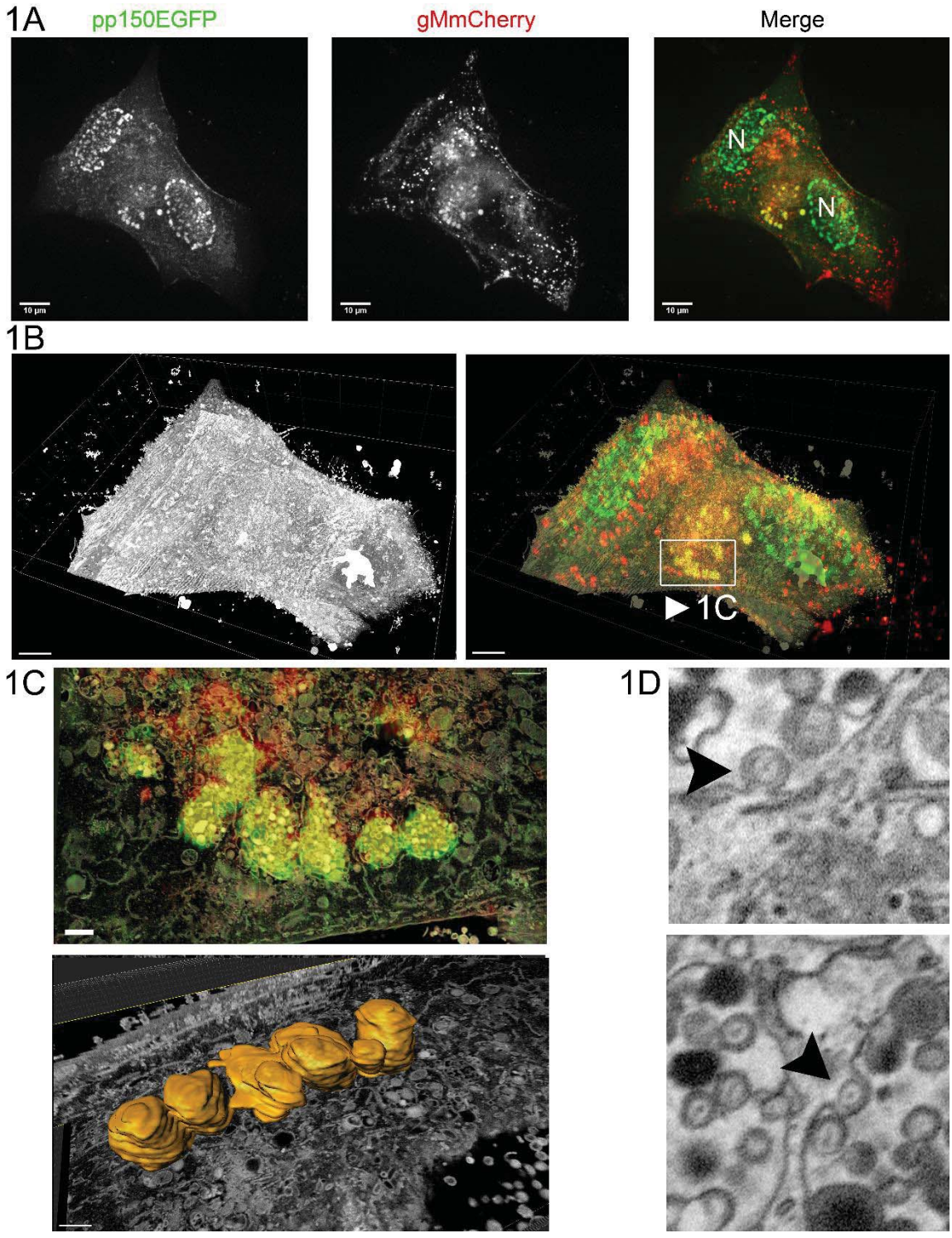

Figure 1. Correlative fluorescence and EM data show large multivesicular bodies filled with virus progeny. CLEM of HFF-Cells infected with HCMV-UL32EGFP-UL100mCherry (MOI 3) at

4dpi. **1A** Maximum z-projection of pp150-EGFP and gM-mCherry signal. Large bodies that contain strong signals of both proteins are located in the cytoplasm. In the merge, N marks nuclei, containing pp150 signal. Scale bar represents 10 µm. **1B** Correlative 3D rendering of the SBF-SEM data corresponding to the cell shown in 1A. The white frame marks MVBs that are also highlighted in 1C and supplementary video 1B. Scale bar represents 7 µm. **1C** SBF-SEM images from MVBs correlated with fluorescence images. Large vesicular bodies contain numerous virus particles. Exemplary surface renderings are shown for the largest bodies in the field of view. Scale bars correspond to 1 µm**. 1D** Enlarged excerpts from the SBF-SEM dataset shown in 1B. The signal is inverted to facilitate comparison with TEM images. Single non-enveloped virus particles were observed budding into the large vesicles. Also, refer to suppl. video 1A-B for a 3D rendering of the presented data.

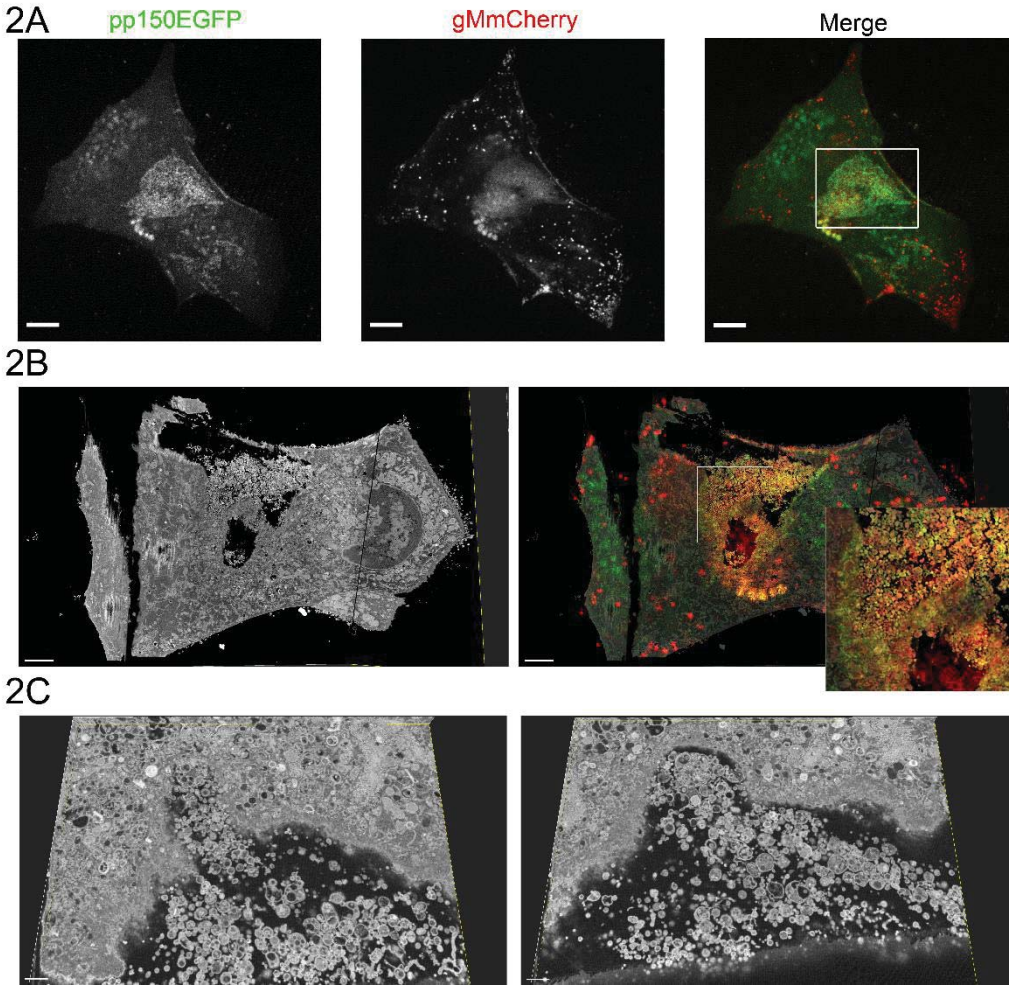

Figure 2. Large VEAs contain viral products and other vesicular material. CLEM of HFF-Cells infected with HCMV-UL32EGFP-UL100mCherry (MOI 3) at 4 dpi. **2A** Confocal section of pp150-EGFP and gM-mCherry signal close to the plasma membrane. Large accumulations of virus particles, marked by the white frame, are seemingly located below the cell. Scale bar represents 10 µm. **2B** SBF-SEM images and correlation to fluorescence data for the area below the cell shown in 1A confirming that VEAs are located outside of the cell. The areas contain numerous virus particles, dense bodies, and other material. Scale bar represents 3 µm. **2C** Details of invaginations that can be found in SBF-SEM data occurring below the cell surface. Scale bars represent 700 nm.

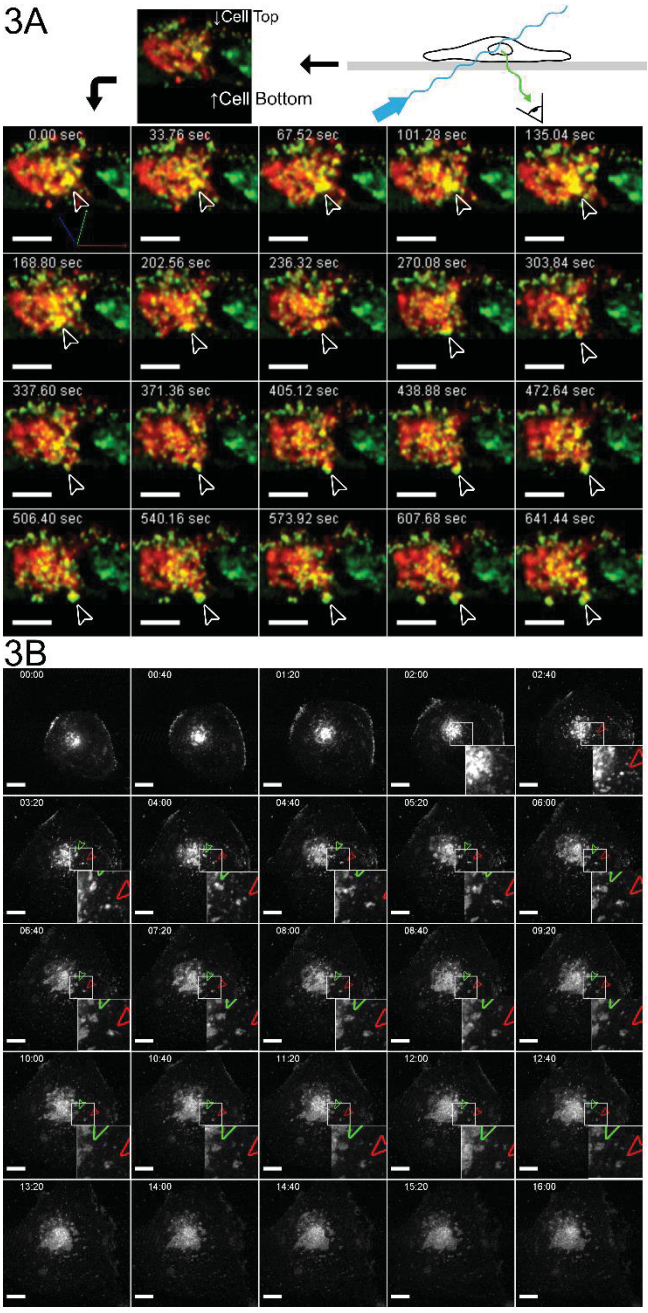

Figure 3. Dynamic information from live infected cells shows bulk release mechanics. 3A HFF cells were infected with HCMV-UL32EGFP-UL100mCherry at an MOI of 1. At 96 hpi the cells were imaged by lattice light-sheet microscopy, taking volumes of whole cells every 2.11 seconds. Shown is a montage of a time-lapse at a single plane at a 30° angle to the growth substrate. Indicated with the white arrowhead is a large body that approaches the plasma membrane and appears to fuse with it. Scale bar represents 5 µm. Also, refer to suppl. video 2 for a rendering and several side views. **3B** HFF cells were infected with HCMV-UL32SNAP-UL100mScalet-I at an MOI of 1. At 72 hpi, cells were imaged live with confocal spinning disk microscopy. Accumulations at the plasma membrane could be observed to originate from large bodies highlighted with colored

arrowheads. Scale bar represents 10 μm. The time format is hh:mm. Also, refer to suppl. video 3 and 4.

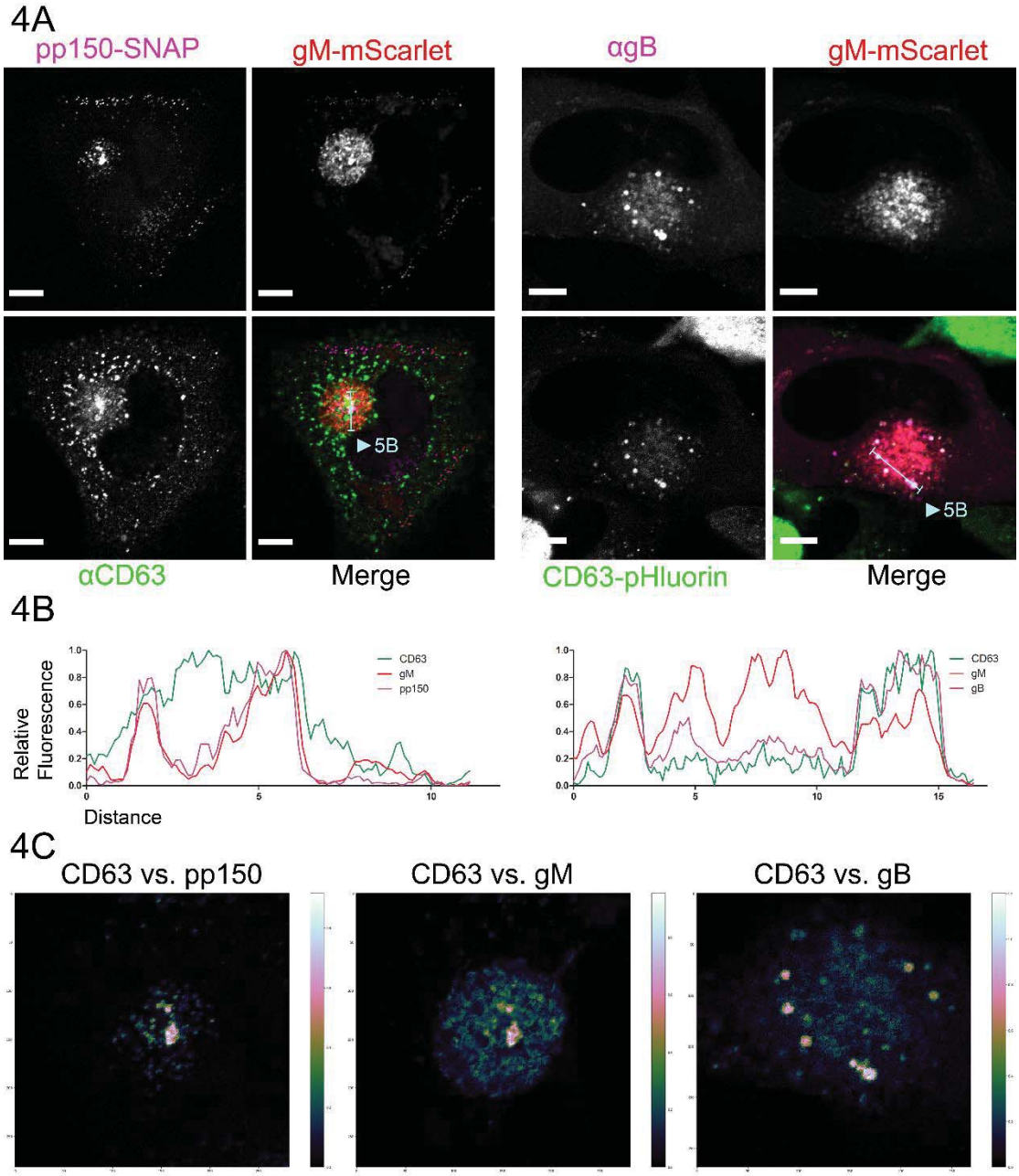

Figure 4. Tetraspanin CD63 colocalizes with gM, gB and pp150. 4A HFF-WT or HFF-CD63pHluorin cells were infected at an MOI of 1 with HCMV-UL32SNAP-UL100mScarlet-I. Cells were fixed at 4 dpi and IF stained for gB (HFF-CD63pHluorin) or CD63 (HFF-WT). The images show representative cells and the localization pattern of CD63 compared to gB, gM, and pp150. CD63 localizes to the assembly complex center and marks larger vesicles in the cytoplasm that are also gB and gM positive. **4B** Line plots for the indicated areas in 5A. A strong colocalization between gM, gB and CD63 can be seen. Colocalization with pp150 is weaker. **4C** Spatial weighted colocalization analysis shows certain areas in the assembly complex where CD63 colocalization with viral molecules is especially pronounced. All scale bars correspond to 10 µm.

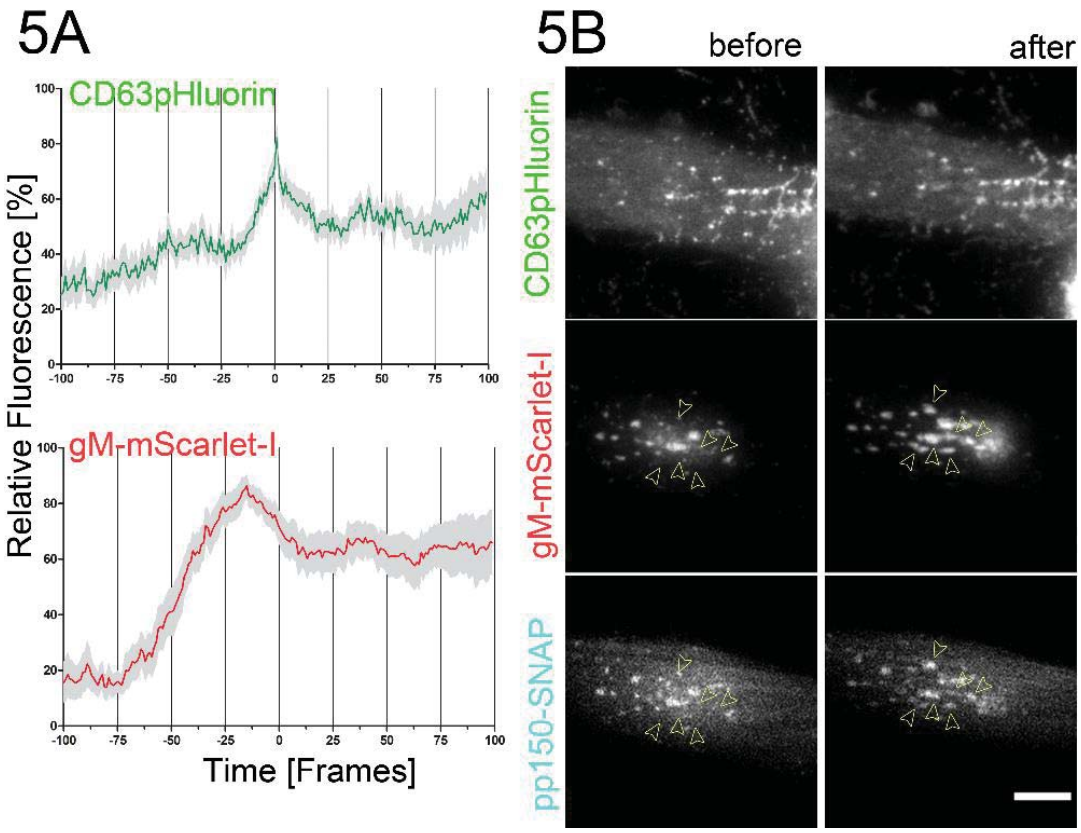

Figure 5. VEAs are the result of fusion events at the plasma membrane. HFF-CD63pHluorin were infected with HCMV-UL32SNAP-UL100mScarlet-I. Cells were imaged at 72 and 96 hpi by fluorescence microscopy in TIRF conditions over time-periods of several hours. **5A** Exocytosis events from putative MVBs are accompanied by a CD63pHluorin flash. A rapid decrease in fluorescence indicates that most of the fluorescent CD63pHluorin quickly diffuses away from the fusion site. The gM signal increases directly before the fusion event and decreases as the round shape relaxes into a flattened patch. The exocytosed material emits the continuously elevated signal. Solid lines are averages from 14 events extracted from 5 cells in 4 replicates. Grey areas show the standard error of the mean. **5B** TIRF images of a cell before and after the fusion events averaged in 5A. Positions that were measured in this particular cell are indicated with the yellow arrowheads. After the fusion-events, VEAs of gM and pp150 can be seen close to the cover glass. All scale bars represent 10 µm.

Table 1. Sequences for 2-Step BAC mutagenesis of HCMV-TB40-UL32SNAP-UL100mScarlet-I.

TB40-UL32-SNAP Insert Sequence	
Insert Sequence	**CACACGGAGGATCCACCGGTCGCCACC atggacaaagactgcgaaatgaagcgcaccaccctg gatagccctctgggcaagctggaactgtctgggtgcg aacagggcctgcacgagatcaagctgctgggcaaag gaacatctgccgccgacgccgtggaagtgcctgcccc agccgccgtgctgggcggaccagagccactgatgca ggccaccgcctggctcaacgcctactttcaccagcctg aggccatcgaggagttccctgtgccagccctgcaccac ccagtgttccagcaggagagctttacccgccaggtgct gtggaaactgctgaaagtggtgaagttcggagaggtca tcagctaccagcagctggccgccctggccggcaatcc cgccgccaccgccgccgtgaaaaccgccctgagcgg aaatcccgtgcccattctgatcccctgccaccgggtggt gtctagctctggcgccgtgggggctacgagggcggg ctcgccgtgaaagagtggctgctggcccacgagggcc acagactgggcaagcctgggctgggt**
TB40-UL100mScarlet-I Primer (50bp overhangs)	
Forward	**ACT ATC ACG TCG TGG ACT TTG AAA GGC TCA ACA TGT CGG CCT ACA ACG TAG TGA GCA AGG GCG AGG C**
Reverse	**CAC ACC AGC TGC ACC GAG TCT AAG AAA AGC ATA GGC GTG TGC AGG TGC ATC TTG TAC AGC TCG TCC ATG CC**

Supplementary Figure 1

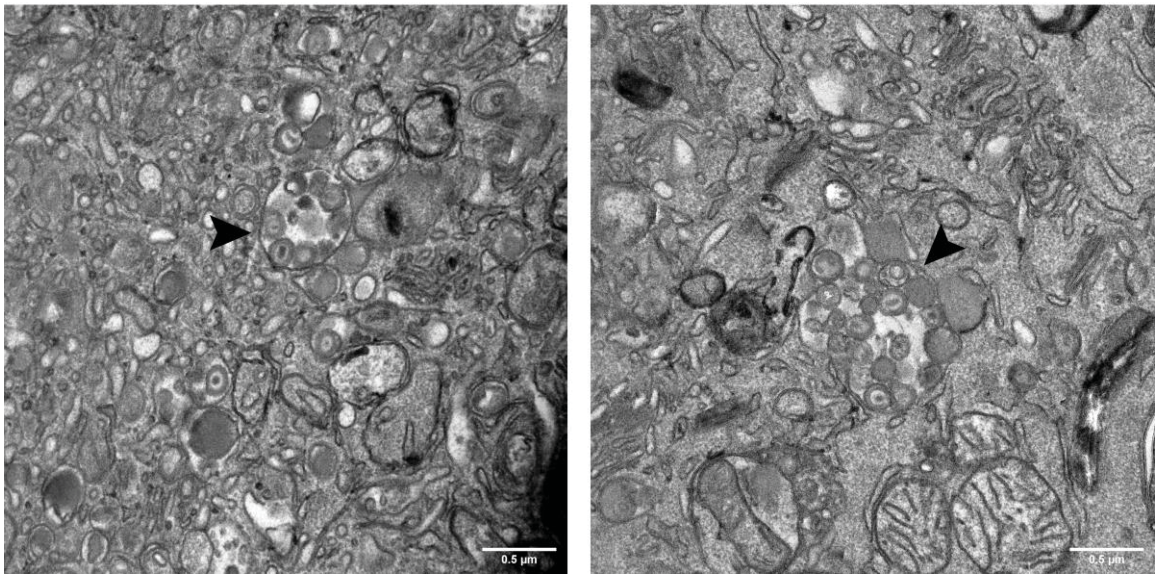

Supplementary Figure 1. MVBs with viral products are not an artifact of the tagged mutant HCMV. HFF-WT cells were infected with HCMV-TB40-WT at an MOI of 5, fixed, and processed for EM as described for SBF-SEM at 120 hpi. Instead of conductive epon used for SBF-SEM, the cells were embedded without fillers for classical sectioning. HCMV-TB40-WT also displays the ability to produce MVBs filled with virus progeny (filled arrowheads). All scale bars represent 0.5 µm.

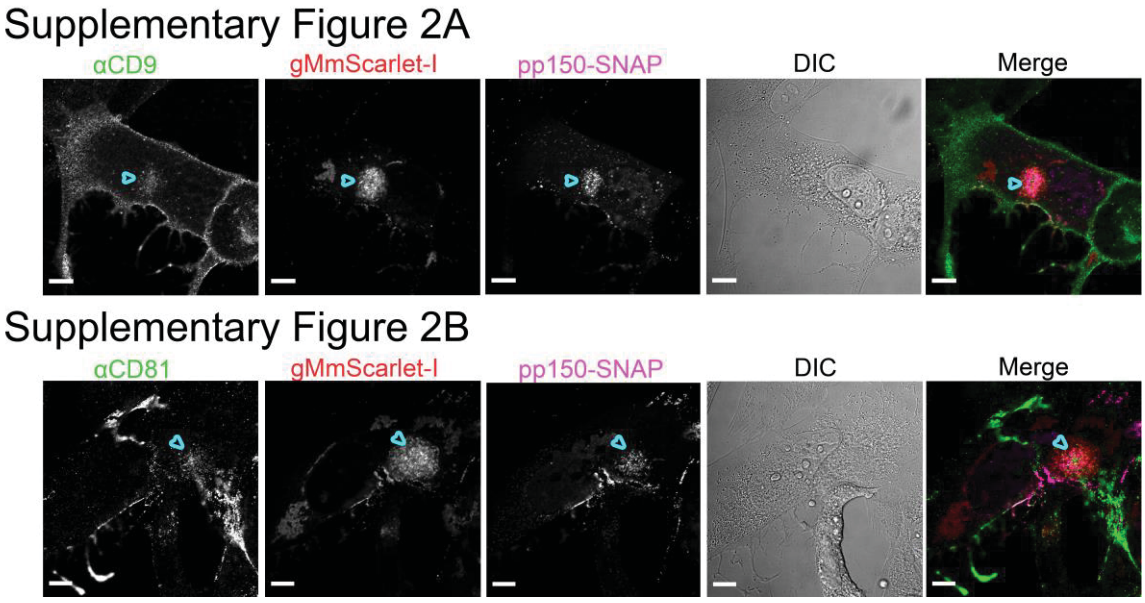

Supplementary Figure 2. Tetraspanins CD9 and CD81 localize to the assembly compartment. **2A-B** HFF cells were infected at an MOI of 1 with HCMV-UL32SNAP-UL100mScarlet-I. Cells were fixed at 4 dpi and IF stained for CD9 and CD81. The images show representative cells and the localization pattern of the CD molecules relative to gM and pp150. CD9 and CD81 localize mainly to the center of the replication compartments as well as the cell surface.

Supplementary Videos 1A and 1B. SBF-SEM rendering of infected HFF cells. The video shows an excerpt from the dataset described in Figure 1. HFF-cells were infected with an MOI of 3 and fixed 4dpi. **1A** Overview rendering of the whole SBF-SEM dataset of the cells shown in Figure 1. **1B** A group of prominent virus-filled MVBs is highlighted by a surface rendering. Several more MVBs are present in the cell.

Supplementary Video 2. SBF-SEM of an area between the cell surface and the growth substrate. The video shows a subset of planes from the dataset described in Figure 2C rendered as a video. Infection conditions are as described before. The signal was inverted to resemble the TEM contrast, which is likely to be more familiar to the viewer. Shown is a large invagination below the cell at the growth substrate. These might resemble fusion events, even though the dynamic information is missing in EM methods.

Supplementary Video 3. Multi-perspective 3D rendering of volumetric time-lapse microscopy data of HCMV release. HFF cell, infected with HCMV-UL32EGFP-UL100mCherry as described in Figure 3A. The video shows from several perspectives how a large MVB positive for UL32EGFP and UL100mCherry traverses the cytoplasm fuses with the plasma membrane. The first seconds show the 3D video, followed by a split-screen part of three different perspectives. A spotlight effect highlights the same body in all three parts. In the left third, the MVB is followed by a moving section, parallel to the growth substrate, through the volume on its way downwards to the lower cell surface. In the middle part, the body is followed as a 3D rendering through the cell. The camera angle moves to keep the body visible, as well as possible. The last third shows how the MVB fuses with the plasma membrane in a static cross-section. Due to the optical setup of the lattice-light-sheet microscope (See Figure 3A), the grid added by Arivis 4D is tilted 30° respective to the real physical orientation of the cell in the microscope.

Supplementary Videos 4 and 5. Live-cell long time-lapse spinning-disc microscopy videos. HFF cells were infected with HCMV-UL32SNAP-UL100mScalet-I at an MOI of 1. At 72 hpi, cells were stained for pp150SNAP and imaged live by spinning disk microscopy. 8-micrometer stacks in 1-micrometer increments were acquired every 40 minutes. The plane shown is the section of the cell closest to the coverglass. Cells can be seen to release virus particles in short intermittent bursts over several hours. Pp150-SNAP labeling is shown in green and gM-mScarlet-I label in red. The time format is hh:mm.

Supplementary Table 1 Mass Spectrometry Results.